Journal of Materials Processing Technology 236 (2016) 138–147

Contents lists available at ScienceDirect

Journal of Materials Processing Technology

journal homepage: www.elsevier.com/locate/jmatprotec

EDM mechanism of single crystal SiC with respect to thermal, mechanical and chemical aspects

Yonghua Zhao [a,*], Masanori Kunieda [a], Kohzoh Abe [b]

[a] The University of Tokyo, Hongo 7-3-1, Bunkyo, Tokyo, 113-8656, Japan
[b] Hamada Heavy Industries Ltd., 272-8, Takaono, Ozu-machi, Kikuchi-gun, 869-1232, Kumamoto, Japan

ARTICLE INFO

Article history:
Received 25 November 2015
Received in revised form 15 April 2016
Accepted 8 May 2016
Available online 10 May 2016

Keywords:
Electrical discharge machining
Single crystal SiC
Material removal mechanism
Heat transfer
Crystallographic structure
Oxidation

ABSTRACT

In this study, electrical discharge machining (EDM), a non-contact thermal machining process, is proposed for machining single crystal silicon carbide (SiC) which exhibits extreme mechanical hardness. However, as a semiconductor, SiC demonstrates significantly different EDM characteristics compared with those of metallic materials. This research clarifies the EDM characteristics of SiC from thermal, mechanical and chemical aspects through experimental and analytical approaches. The heat transfer analysis of a single discharge of SiC taking into account Joule heating effect revealed that Joule heating effect can increase the surface temperature of SiC near the discharge spot considerably. On the other hand, experimental investigations on the EDM of SiC found that brittle fractures along crystal orientations occur in the EDM of SiC due to thermal shock. However, the influence of the crystal anisotropy of SiC on the EDM characteristics was not significant. Finally, the EDM mechanism of SiC was investigated from chemical aspects. Oxidation reaction was confirmed in the EDM of SiC in deionized water. All of these factors helped improve the machining rate of SiC to a certain extent.

1. Introduction

Single crystal silicon carbide (SiC) is an extremely hard and inert IV–IV compound semiconductor material with a hexagonal close-packed crystal structure. It is a well-known semiconductor which has been drawing special attention in recent years because of its high suitability for high-temperature, high-power, high-frequency semiconductor devices, whereas conventional semiconductors such as Si, GaAs etc. are reaching their limits (Dhanaraj et al., 2010). This is because SiC possesses superior electrical and physical properties over Si, such as a wider band-gap (three times that of Si), larger critical electric field intensity (10 times that of Si), higher thermal conductivity, higher electron saturation drift velocity, etc. Furthermore, SiC devices can reduce power loss and allow downsizing of various power supply units and power conversion equipments. However, it meets great challenges to scale out the application of SiC devices due to its high cost. According to Friedrichs et al. (2010), currently Si is still dominating nearly all semiconductor applications for economic reasons and SiC has little chance of being widely used unless its cost can be reduced to that of Si, or lower.

There are mainly two reasons for the high manufacturing costs of SiC wafers. One is that, SiC has high brittleness due to its crystal structure. On the other hand, SiC crystals exhibit very high bonding energy owing to the short interatomic distance of Si–C (0.189 nm), resulting in the extreme hardness of SiC, as shown in Table 1 (Matsunami et al., 2011; Emsley, 1998). The extreme hardness and brittleness make SiC a difficult-to-machine material by mechanical machining approaches. For example, with the SiC wafer slicing process using multi-wire saw, this is a traditional mechanical machining process conventionally used for slicing Si wafers, and it is significantly time- and cost- consuming when applied to the wafering of SiC ingots. Moreover, since the hardness of SiC is close to that of diamond, diamond is the only tool which can machine SiC, further increasing the machining costs of SiC.

On the other hand, electrical discharge machining (EDM) is a non-contact thermal machining process which can machine any conductive material regardless of the workpiece hardness as the material removal is based on melting and/or evaporating the material. Therefore, EDM is recently applied to machine SiC to reduce costs and improve the machining efficiency and accuracy. Several researches on the EDM of silicon carbide ceramic which is similar to silicon carbide single crystal in terms of hardness and brittleness have been carried out in the past. Saeki et al. (1996) investigated the material removal mechanism of high-resistivity material (Si_3N_4-SiC ceramics) in EDM by calculating the workpiece temperature

* Corresponding author.
E-mail address: yonghua.zhao@edm.t.u-tokyo.ac.jp (Y. Zhao).

http://dx.doi.org/10.1016/j.jmatprotec.2016.05.010
0924-0136/

distribution and found that Joule heat caused temperature to rise near the discharge spot. Luis et al. (2005) conducted sinking EDM of siliconized or reaction-bonded silicon carbide (SiSiC) and investigated the influence of the most relevant EDM factors on material removal rate and electrode wear. Liu et al. (2008) applied electrical discharge milling to machine silicon carbide ceramic to improve the machining efficiency and their experimental result showed that the machining rate can be improved to a certain extent compared to mechanical machining process but not enough to meet industrial demands. Ji et al. (2011) investigated the electrical discharge milling performance of SiC ceramics by varying machining conditions and they concluded that the removal mechanism of EDM of SiC ceramic consisted of material melting, evaporation and thermal spalling. In order to improve the machining efficiency furthermore, Ji et al. (2010, 2013) developed an electrical discharge milling and mechanical grinding compound process and investigated the surface integrity after machining. All of the researches described above are focused on SiC ceramic. With regard to SiC single crystal, Kato et al. (2009) succeeded in the wire EDM slicing of 2inch 4H-SiC wafer and discovered that wire EDM is suitable for slicing SiC wafer with high efficiency and low damage. Yamada et al. (2012) revealed that wire EDM can achieve higher cutting speed, smaller surface roughness, smaller warpage and smaller kerf loss than the diamond wire saw for wafering SiC ingots. Ishikawa et al. (2014) investigated the cross-section of as-sliced 6H-SiC by transmission electron microscopy (TEM) and found that little crystal disorder was induced in hexagonal SiC after EDM. Kitamura et al. (2013) carried out EDM experiments of SiC wafer in oil and observed the discharge gap phenomenon taking advantage of the optical transparency of SiC wafer. The research found that the discharge gap of EDM of SiC during machining is mostly occupied by bubbles. Zhao et al. (2014) investigated the optimal machining conditions for EDM of 4H-SiC and proposed the foil EDM method for slicing SiC wafers which uses a foil tool electrode. However, no sufficient study has been carried out on the EDM mechanism of SiC. Zhao et al. (2015) also developed a multiple discharge EDM coring method utilizing the electrostatic induction feeding method to achieve high efficiency coring of 4H-SiC ingots and wafers. In order to reduce tool wear and improve the machining rate of SiC, Yan and Tan (2015) developed a hybrid sintered diamond tool for the micro-machining of SiC which combines EDM and grinding process, and succeeded in achieving a nanometer-scale surface finish. Furthermore, Okamoto et al. (2012) conducted research on the development of a multi-wire electrical discharge slicing equipment for slicing multiple SiC wafers simultaneously by EDM in order to reduce the time cost and manufacturing cost of SiC wafers. The multi-wire EDM slicing process has been progressing rapidly in recent years. Itokazu et al. (2014) realized the simultaneous slicing of 100mm-square poly-crystal SiC material by 40 times without wire break by the multi-wire EDM method, which confirmed the feasibility and potentials of applying EDM for machining SiC. Ogawa et al. (2014) succeeded in the multi-wire EDM slicing of 4 inch SiC balk single crystal with the developed electrical discharge pulse control system to prevent wire break during machining. However, as discussed above, to date most literature reports focused on the application, whereas the material removal mechanism of SiC in EDM, which is of great importance for improving the machining performance, has not been comprehensively investigated. Since the physical properties of SiC and metallic material (in this study cold tool steel SKD11 was used), as described in Table 1, differs considerably, it is of significant importance to clarify the EDM mechanism of SiC. Therefore, in this study, first a comparative study between the EDM of SiC and metallic material was carried out. Then based on the differences in the EDM of the two materials, the thermal, mechanical and chemical removal mechanism of the EDM of SiC were investigated and discussed respectively.

Table 1
Comparison of material properties between SiC, Si and steel.

	SiC	Si	SKD steel
Knoop hardness [kgf/mm^2]	2400–3000	560–710	–
Electrical resistivity [Ω cm]	2×10^{-2}	$< 2 \times 10^{-2}$	1.5×10^{-5}
Melting point [°C]	–	1410	1540
Sublimation point [°C]	2000–2200 °C	–	–
Thermal conductivity [W m^{-1} K^{-1}]	490	148	40

Table 2
Pre-set wire EDM conditions for machining SiC and SKD11.

Wire electrode	Brass wire, ϕ200 μm
Workpiece polarity	(+)
Dielectric liquid	Deionized water
Machining length	10 mm
Workpiece thickness	10 mm
Duty factor	9.1%

2. Differences in EDM characteristics between SiC and tool steel

EDM is generally applied to machine metallic material. However, SiC differs from other metallic materials with its higher electric resistivity and higher thermal conductivity, as shown in Table 1. In order to clarify the differences in EDM characteristics between SiC and other metallic materials, comparative experiments between the wire EDM of SiC and cold tool steel were conducted. The machining conditions were pre-set the same as shown in Table 2. The experimental results of the material removal rate (MRR) differences between the two materials are shown in Fig. 1, where t_e indicates the measured discharge duration in machining. The points connected by the dashed lines indicate the same preset machining conditions. The figure indicates that under the same machining conditions, the measured discharge current in the EDM of SiC is much lower than that of steel due to the higher resistivity of SiC. The material removal volume per single discharge of SiC material, however, was several times higher than that of steel under the same discharge current. In addition, according to the previous study carried out by Zhao et al. (2014), the machined surface roughness and kerf loss were also much larger in the case of SiC than steel.

However, in theory, according to the study on the effects of material properties on EDM rate conducted by Yamashita et al. (2011), SiC is categorized as difficult-to-machine material by EDM due to its extremely high thermal conductivity and high sublimation point. With regard to the reasons for the differences, three aspects are investigated: thermal factor, mechanical factor and chemical factor, as shown in the following.

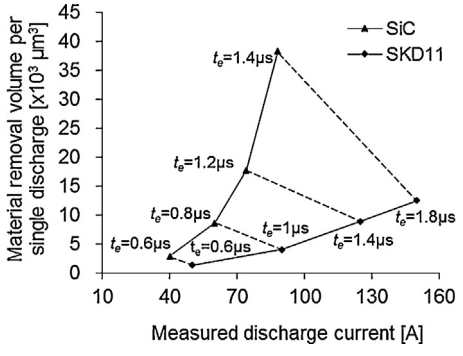

Fig. 1. Difference in material removal rate by EDM between SiC and steel.

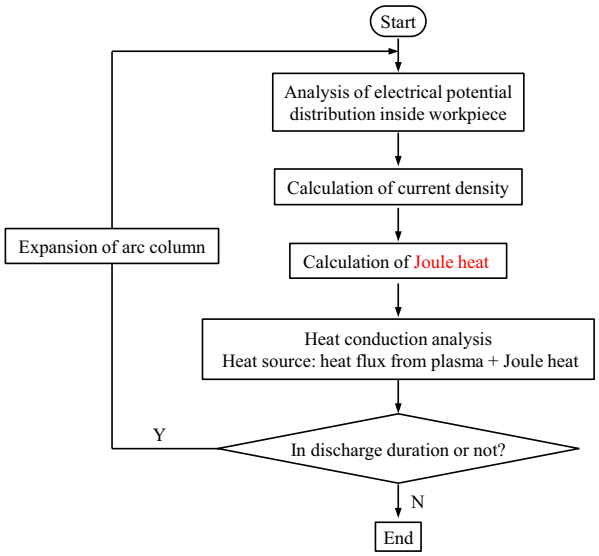

Fig. 2. Flow chart of calculation of temperature distribution inside SiC workpiece.

3. Thermal aspects

This section demonstrates the difference in temperature distribution resulting from a single discharge between SiC and steel due to their different thermo-physical properties, and clarifies the reasons for the difference in the material removal rate. Since it is impossible to obtain 3-dimensional temperature distribution inside the workpiece by experiments, the temperature distribution was calculated by solving heat conduction equation. The finite difference method (FDM) was employed to perform the heat conduction analysis. In addition, Joule heating was taken into consideration in the calculation. This is because, according to the research by Rich (1961), Joule heating is comparable to the energy input from arc plasma for the high-resistivity materials.

3.1. Analysis algorithm

Fig. 2 shows the analysis procedure for calculating the temperature distribution. First, the electrical potential distribution inside the workpiece is computed considering the resistivity. Based on the calculated electrical potential distribution, the current density distribution inside the workpiece is calculated. The generation of Joule heat is then calculated based on the obtained current density and workpiece resistivity. Next, considering the energy input from both the Joule heat and heat flux from discharges, heat conduction analysis is carried out to compute the time-dependent temperature distribution in workpiece. To achieve accurate calculation, the changes in the arc column diameter with time due to the expansion behaviour of the arc plasma, which will be explained later, is taken into consideration at every time step.

Table 3
Material properties used for simulation.

		SiC	SKD11
Specific heat	[J/(kg K)]	656	469
Density	[kg m^{-3}]	3210	7850
Latent heat for fusion	[kJ kg^{-1}]	–	267
Latent heat for vaporization	[kJ kg^{-1}]	–	6285

3.2. Analysis model

The analysis model used in the study is shown in Fig. 3. Considering that current and heat flow axis-symmetrically into the workpiece, a cylindrical workpiece model was used. Kojima et al. (2008) measured the arc plasma diameter in EDM by spectroscopic measurement method and found that the plasma diameter changes with time during discharge. For this reason, in this study, a circular disk with a time-dependent diameter $d(t)$ was used as the model of arc plasma column (energy source). The arc column is set right above the center of the workpiece working surface. As the whole model is axisymmetric, it can also be simplified to a two-dimensional model, as shown in Fig. 3(b). The center brown area on the working surface indicates the energy input region where the current density j and heat flux q'' are assumed to be uniform. To perform the finite difference method, the analysis model is meshed monotonously in both the radial and longitudinal directions.

As supplementary information for Table 1, the necessary thermo-physical properties for the analysis are listed in Table 3. For comparison, both SiC and SKD steel are included in the table. For simplicity, the dependency of the material properties on temperature is not considered here. In addition, the removal of material by melting and evaporation after the temperature exceeds the melting point is not considered in the analysis. The latent heat for fusion and vaporization of the steel material, as shown in Table 3, is taken into account in the analysis. The latent heat for the decomposition of SiC was not considered due to the lack of relevant data.

3.3. Calculation of Joule heat

When an electric current passes through a conductor, heat is released from the conductor, which is called Joule heating effect. To calculate the generation of Joule heat in SiC workpiece in EDM, the electrical field must be determined first. The electrical potential distribution can be calculated based on the law of charge conservation.

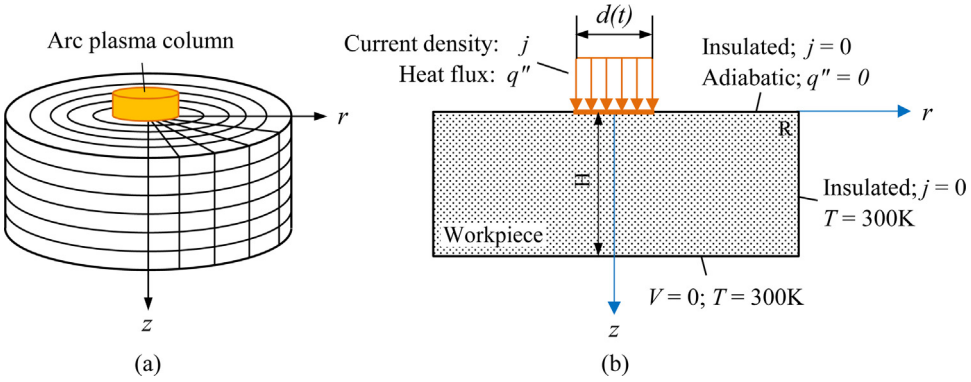

Fig. 3. Illustration of electric potential and heat transfer analysis models.

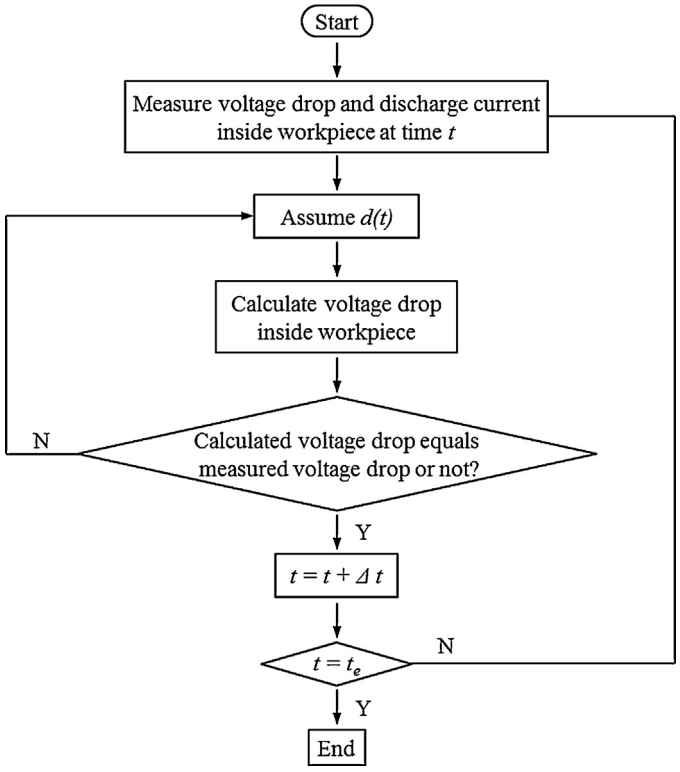

Fig. 4. Procedures for inverse solution of plasma diameter in EDM of SiC.

The boundary conditions for the analysis are noted in Fig. 3. The electrical potential V at the nodes on the bottom surface of the workpiece is set as zero (ground level). Except for the energy input region, all the other surfaces are considered to be insulated. The current density j inside the arc column is assumed to be uniform in the whole discharge area for simplicity, which equals the value of current divided by the cross-section area of the arc column as expressed in Eq. (1). Here, i_e refers to the discharge current and $d(t)$ is the time-dependent diameter of are plasma.

$$j = \frac{i_e}{\pi(d(t)/2)^2} \quad (1)$$

In Eq. (1), $d(t)$, which has a significant influence on the current density j, should be decided correctly. In some cases, for simplicity, Eq. (2), obtained by Saito and Kobayashi (1967) assuming that heat source diameters were equal to discharge craters diameters measured in experiments, is used as the energy source diameter.

$$d(\mathrm{t}) = 2.4 \times 10^{-3} \times t^{0.4} \times i_e^{0.4} \quad (2)$$

Here the units of $d(t)$, t, and i_e are [m], [s], and [A] respectively. Kitamura and Kunieda (2014) observed the arc plasma using a high speed video camera and found that the diameter of the arc plasma was much larger than that of the discharge crater. However, since $d(t)$ depends on gap width and pulse conditions, the $d(t)$ obtained by Kitamura and Kunieda (2014) cannot be used for the present study. Hence, in this paper, the correct heat source diameter in the EDM of SiC was obtained by solving the inverse problem of electrical potential analysis proposed by Saeki et al. (1996).

3.3.1. Inverse solution of plasma diameter in EDM of SiC

Fig. 4 shows the flowchart of the calculation of the plasma diameter. At the start, the actual discharge current and voltage waveform of EDM of SiC are measured through experiments. Based on the measured discharge voltage and current, the voltage drop inside SiC at a certain time t (here t refers to the passage of time) after discharge ignition and the corresponding discharge current can be obtained. In the iteration of the program shown in the flowchart, the arc column diameter, $d(t)$, is set to be changing from 0 to 200 μm with an interval of 0.01 μm. At each assumed value of $d(t)$, the voltage drop inside SiC is calculated. At a certain time t, if the calculated voltage drop inside SiC agrees with the measured value, the assumed $d(t)$ will be taken as the plasma diameter at time t. By repeating the program, $d(t)$ at different times can be calculated. Saeki et al. (1996) used this method to obtain the expansion of arc column with time lapse in EDM of ceramics through experiments.

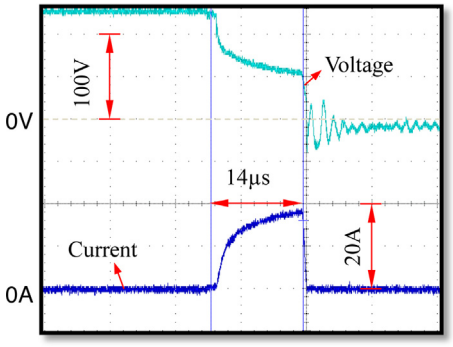

Fig. 5. Discharge waveform of SiC by sinking EDM.

The discharge waveforms of SiC measured through experiments are shown in Fig. 5. Table 4 shows the experimental conditions for measuring the discharge waveforms. The measured discharge gap voltage U_m is composed of three parts: voltage drop in tool electrode U_t, voltage drop in arc plasma U_e and voltage drop inside workpiece U_w due to the resistivity of workpiece, as shown in Fig. 6. The voltage drop in the copper tool electrode and workpiece made of metallic material is very small because they are good conductors, and therefore can be neglected. The discharge voltage measured in the EDM of steel is usually considered the voltage drop in arc plasma. Hence, the voltage drop in the workpiece of SiC was obtained by subtracting the measured discharge voltage of steel from that of SiC under the same discharge current, as illustrated in Fig. 6(b).

Based on the method described above, the plasma diameter $d(t)$ was calculated under the conditions shown in Table 4, as shown in Fig. 7. The approximate curve is used to express the change in the arc plasma diameter with time.

3.3.2. Joule heat

Based on the law of charge conservation, the electrical potential distribution in SiC was calculated. Fig. 8 shows the analysis results of electrical potential distribution inside SiC at $t = 2$ μs after discharge when the discharge current is around 14A and the plasma diameter is around 27 μm. It can be seen that the voltage drop inside SiC, around 40 V, mostly occurred in the vicinity of the discharge spot where the current density is highest.

Table 4
Experimental conditions for measuring the discharge waveform of SiC.

Tool electrode	Copper rod, ϕ5 mm
Workpiece	4H-SiC wafer
Open voltage [V]	120
Preset discharge current [A]	30
Discharge duration [μs]	10
Discharge interval [μs]	2500
Servo voltage [V]	100
Dielectric liquid	EDM oil

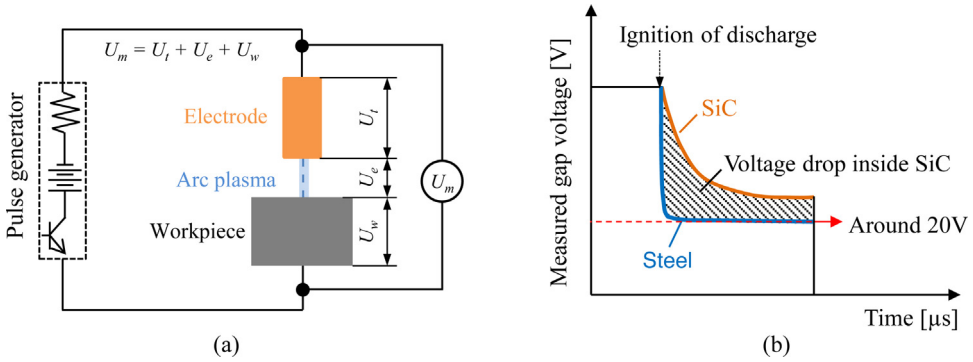

Fig. 6. Measurement of voltage drop inside SiC workpiece in EDM.

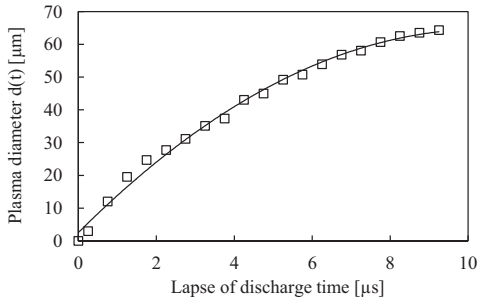

Fig. 7. Time-dependent plasma diameter obtained by solving inverse problem.

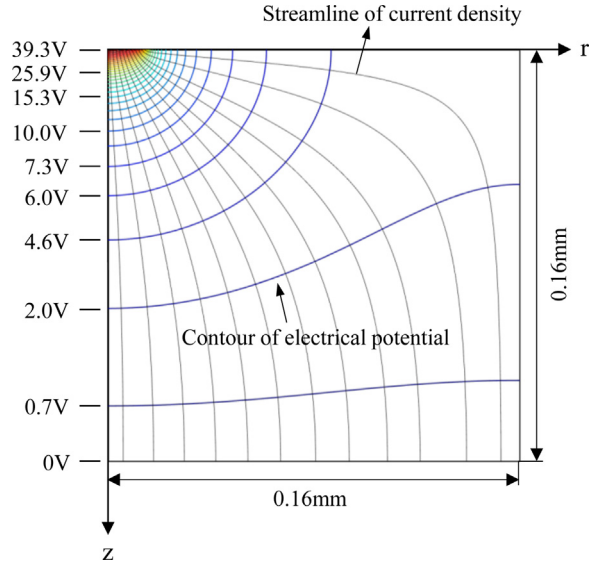

Fig. 8. Electrical potential distribution and current in SiC body at $t = 2$ μs.

The rate $\dot{q}$ at which energy is generated per unit volume of the medium (W/m^3) owing to the Joule heating effect can be calculated based on Joule's law as expressed in the following equation:

$$\dot{q}(r, z, t) = \rho \times j^2 \tag{3}$$

where ρ is the specific electrical resistivity (Ω m) and j the current density (A/m^2) flowing through the conductor.

3.4. Temperature distribution

The temperature distribution inside workpiece can be calculated by solving the time-dependent heat conduction equation in the cylindrical model as expressed in the following:

$$\rho_d c \frac{\partial T(r,z,t)}{\partial t} = \frac{1}{r}\frac{\partial}{\partial r}\left(\lambda r \frac{\partial T(r,z,t)}{\partial r}\right) + \frac{\partial}{\partial z}\left(\lambda \frac{\partial T(r,z,t)}{\partial z}\right) + \dot{q}(r,z,t) \tag{4}$$

where, ρ_d is the density of the workpiece (kg/m^3), c the specific heat (J kg^{-1} K^{-1}), λ the thermal conductivity of the workpiece (W m^{-1} K^{-1}), and T the temperature (K).

The initial temperature T_0 of all the nodes and the ambient temperature T_m in the model were set as room temperature (300 K). The top surface of the workpiece was considered to be adiabatic except for the discharge area, as shown in Fig. 3. All the other surfaces of the workpiece were maintained at room temperature. Material removal was not considered in the analysis for simplicity.

The workpiece polarity was set as anode. It was assumed that the heat flux q'' from arc plasma flows uniformly into the workpiece within the discharge area. Taking the discharge current to be i_e and discharge voltage u_e, the heat flux can be expressed by the following equation, where η is the ratio of the discharge energy distributed into the anode.

$$q'' = \frac{\eta \times u_e \times i_e}{\pi(d(t)/2)^2} \tag{5}$$

In this research, the discharge energy distribution ratio into SiC was not experimentally measured. However, since the thermal conductivity of 4H-SiC (490W m^{-1} K^{-1}) is close to that of copper (401 W m^{-1} K^{-1}), the energy distribution ratio of SiC (anode) η was set as 40% referring to that of copper obtained by Xia et al. (1996). Based on the boundary conditions and Eq. (4), the temperature at every node was calculated making use of the numerical method of finite difference with central difference and explicit method.

3.4.1. Influence of Joule heating effect on temperature distribution

Fig. 9 shows the calculation results of the temperature distribution inside workpiece at $t = 2$ μs with and without taking into consideration the Joule heating effect. When Joule heating effect is not taken into consideration, the surface temperature of SiC at discharge spot drops to 2069 K at $t = 2$ μs after discharge ignition. On the other hand, the surface temperature of SiC at the discharge spot increases significantly to about 4268 K when Joule heating effect is taken into consideration, which indicates that the Joule heating effect contributes considerably to the increase in the surface temperature of SiC in EDM.

3.4.2. Temperature decrease with passage of time

Fig. 10 shows the decrease in the peak temperature at $r = z = 0$ (heat source center on the working surface) with the lapse of time

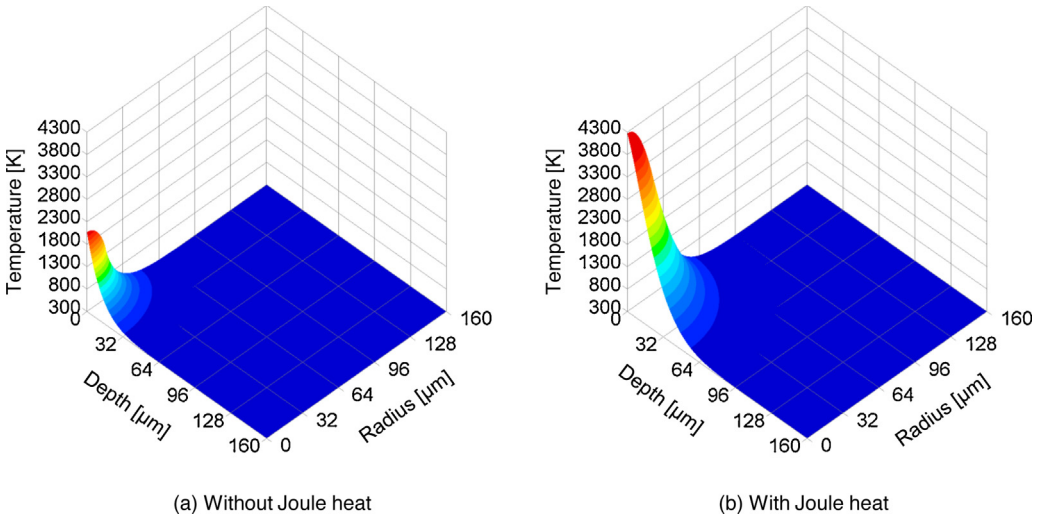

Fig. 9. Calculated temperature distribution in SiC at $t = 2$ μs.

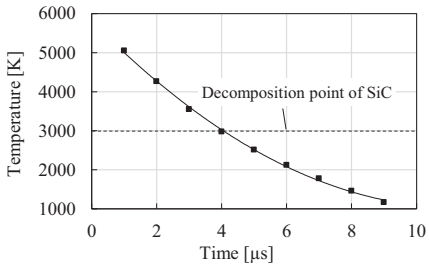

Fig. 10. Change of peak temperature on working surface of SiC with passage of discharge time.

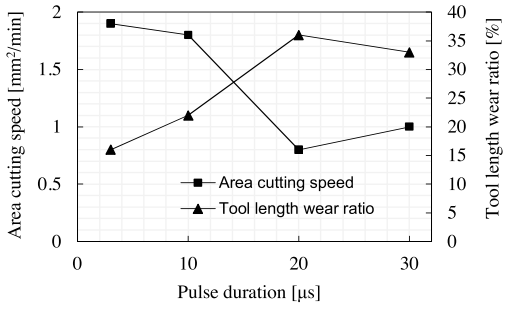

Fig. 11. Influence of pulse duration on EDM of SiC.

after the ignition of discharge. It can be seen that the peak temperature drops below the decomposition temperature, 3000 K, of SiC in about 4 μs due to the high thermal conductivity of SiC and the expansion of heat source diameter. This suggests that a long pulse duration may not contribute to improving the material removal rate of SiC.

To verify this conclusion, experiments were conducted on the sinking EDM cutting of SiC using rectangular shape copper foil tool electrodes to investigate the influence of the pulse duration on the EDM of SiC. Fig. 11 shows the experimental results. It can be seen that with the same duty factor, the machining rate decreases and the tool wear ratio increases with increasing the discharge duration. By repeating machining trials in the experiments, it was confirmed that under either plus or minus polarity, long pulse duration easily results in concentrated discharge and machining becomes extremely unstable. The experimental result validated the analysis result. It was therefore concluded that long pulse duration is not efficient for the EDM of SiC.

3.4.3. *Comparison of single discharge EDM between SiC and SKD11*

The difference in temperature distribution between SiC and SKD11 was investigated to clarify the reasons for the difference in the machining rate shown in Fig. 1.

The same heat source diameter and discharge current were used in the analysis. Fig. 12 (a) and (b) show the analysed results of temperature distribution in SiC and steel, respectively, at time $t = 1$ μs. The peak temperature at the heat source center on the discharge surface of SiC was lower as compared to that of steel due to its higher thermal conductivity. The area of high temperature region of SiC, however, was much larger than that of steel due to the Joule heating effect inside SiC, which helps to increase the average temperature of the working surface in consecutive discharges. Moreover, the area of high temperature region which exceeds the sublimation/decomposition point of SiC was several times larger than the area of high temperature region of steel which exceeds the melting point of steel. In other words, the Joule heating effect is thought to create a larger high temperature (over sublimation point) region on the SiC workpiece surface than steel, contributing to the improvement of the material removal rate of SiC.

On the other hand, it should be noted that in actual machining with the same machining conditions, the heat flux input into SiC and steel is probably different. In the case of SiC, since the discharge voltage is high, under the same servo voltage, the discharge frequency should be high (Kunieda, 2014). This means that the discharge gap width should be smaller than that of steel in order to achieve a higher discharge frequency. According to the findings by Kojima et al. (2008), a smaller discharge gap width will result in a smaller plasma diameter, which consequently brings about a higher heat flux in the EDM of SiC compared with that of steel. This probably is another reason for the higher material removal rate of SiC.

4. Mechanical removal of material in EDM of SiC

Given that SiC is a typical fragile material, the material removal mechanism in EDM may differ significantly from ductile metallic material. In this section, we consider the material removal mechanism of SiC from the perspective of brittle fracture and investigate the influence of crystal structure on the EDM performance.

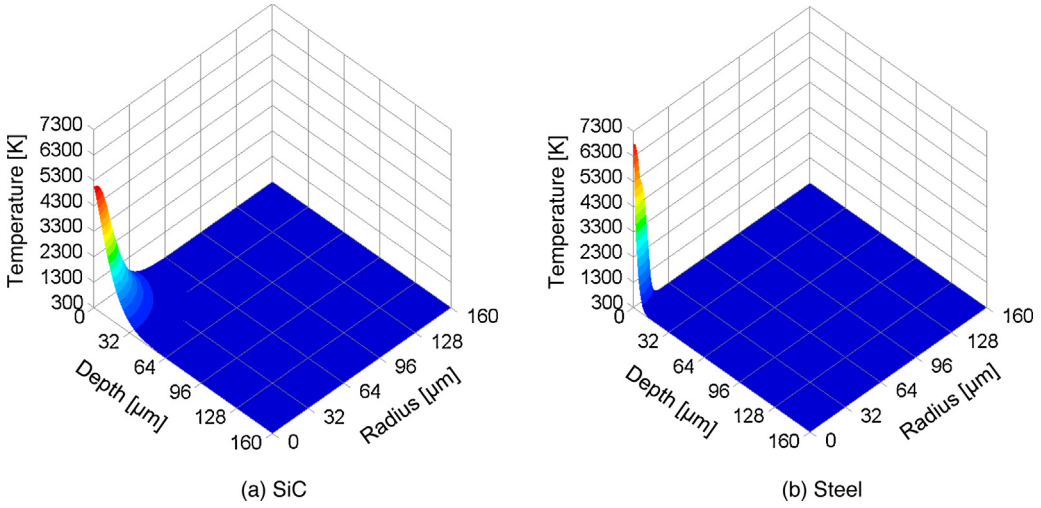

Fig. 12. Comparison of temperature distribution between SiC and steel by single discharge (t = 1 μs).

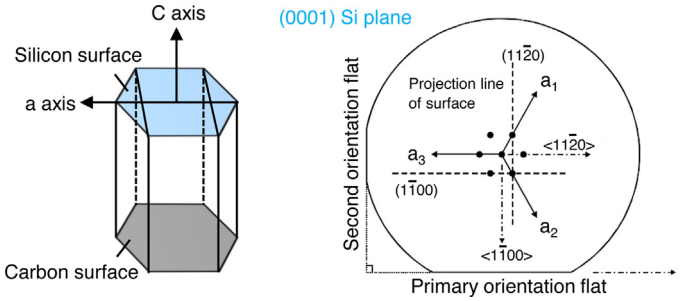

Fig. 13. Crystal orientations and crystal planes of 4H-SiC.

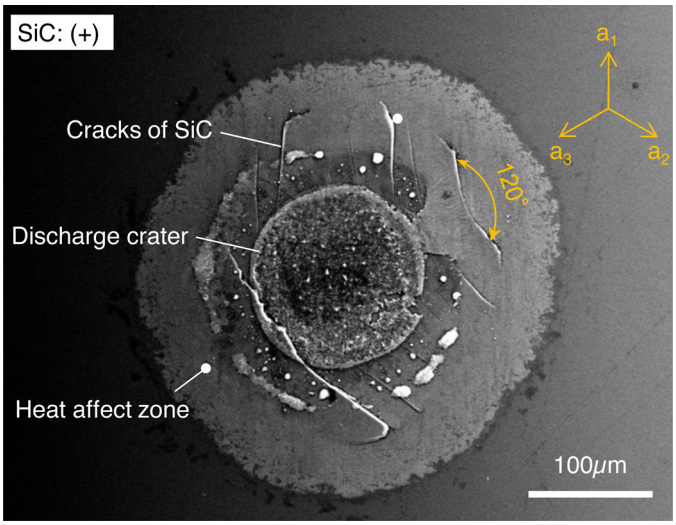

Fig. 14. Cracks in SiC caused by single discharge (i_e = 20A, t_e = 100 μs).

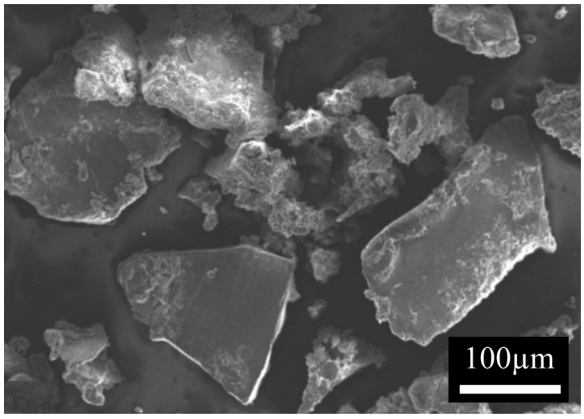

Fig. 15. SEM image of EDM debris of SiC (i_e = 14A, t_e = 10 μs).

4.1. Thermal fracture in EDM of SiC

4H-SiC exhibits a hexagonal close-packed crystal structure, of which the main crystallographic orientations and planes are shown in Fig. 13. The *c* axis marked in the figure refers to the crystal growth axis of SiC. As an extremely brittle material, SiC has a low fracture toughness. Syvajarvi et al. (2000) reported that SiC has two preferred cleavage planes: the (11–20) and (1–100) plane respectively, and cleavages along the crystal plane (1–100) are more reproducible. In the EDM of SiC, due to the existence of temperature gradient resulted from discharge heat, thermal stress is generated inside SiC, which can cause thermal cracks. This consideration was confirmed by the observation of a single discharge crater of SiC, as shown in Fig. 14. Multiple cracks aligned along the crystal orientations of SiC due to thermal shock can be seen clearly.

Micro cracks may cause fracture of SiC workpieces in case of consecutive discharges due to excessive thermal shock. Based on this assumption, EDM experiments were conducted on SiC in clean deionized water in a clean tank by sinking EDM. The EDM debris was collected after experiments and observed using a scanning electron microscope (JEOL JSM-6010LV). The observed image of EDM debris of SiC, shown in Fig. 15, revealed the presence of multi-angular SiC debris particles due to the brittle fracture of SiC. This result coincided with the material removal mechanism of spalling in the EDM of brittle ceramics due to high thermal shock reported by Lauwers et al. (2004). The multi-angular debris particles had nearly hexagonal or square shapes with crystallographically oriented sharp edges. This is considered to be another mechanism causing the higher material removal rate in the EDM of SiC compared to that of steel.

On the other hand, the higher the current density, the higher the heat flux will become, which will increase the thermal stress in the workpiece and cause stress cracks to form more easily. From this point of view, it is considered that optimal machining condi-

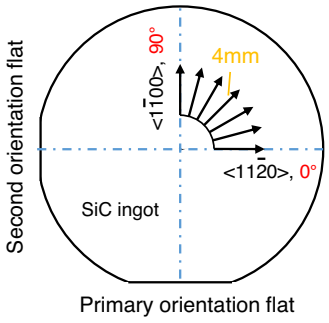

Fig. 16. Illustration of wire EDM cutting of SiC ingot along different crystal orientations.

Table 5
Machining conditions for wire EDM cutting of SiC ingot.

Workpiece	SiC ingot
Workpiece thickness [mm]	18
Wire electrode	Brass wire, ϕ200 μm
Discharge duration [μs]	0.6
Discharge current [A]	56
Dielectric liquid	Deionized water
Specific resistance of dielectric [Ω cm]	106000
Flushing method	Submerging + flushing
Nozzle position to workpiece	Close

tions should be selected in the EDM of single crystal SiC in order to balance the material removal rate and prevent cracks and fractures.

4.2. Influence of crystal structure on machining characteristics

Since thermal cracks tend to propagate along the crystal orientations of SiC, the influences of the crystal structure on the EDM characteristics of SiC was investigated. According to a study by Kawakami and Kunieda (2005), the machining speed depended significantly on the crystal orientation in the micro-EDM process of monocrystalline tungsten under finish-machining conditions. Therefore, experiments of wire EDM cutting of 4H-SiC ingot along different crystal orientations, as illustrated in Fig. 16, were conducted. Defining the crystal direction <11–20> and <1–100> as 0° and 90° respectively, SiC ingot was cut every 7.5° in between the two directions to investigate the difference in machining rate. The experimental conditions are shown in Table 5. Fig. 17 is a schematic diagram of the experimental setup. Since the off-axis angle of the SiC wafer surface orientation was 4° ± 0.5°, before the experiment, the SiC ingot was intentionally positioned to make the crystal axis, *c*, parallel to the wire electrode. Machining was conducted by servo feeding the workpiece to the wire electrode. To obtain accurate results, the workpiece feed speed should be properly selected. This

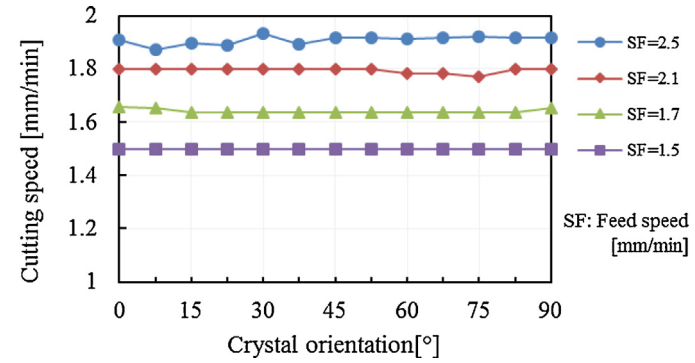

Fig. 18. Wire EDM cutting speed variation with varying cutting directions.

is because, an excessively high feed speed will cause instability of machining due to insufficient gap width. On the contrary, an excessively low feed speed will impose restrictions on the maximum machining speed. In order to reduce the influence of feed speed on the machining rate, stable machining conditions for wire EDM of SiC were first investigated through machining trials before the experiments. The experiments were then conducted near the areas where machining conditions are stable.

The experimental results shown in Fig. 18, however, indicated no obvious variation with varying cutting directions under different servo feed speeds, suggesting that the influence of the anisotropy of crystal orientation in the *c* surface (⊥*c* axis) on the machining rate is negligible in the rough EDM of SiC.

On the other hand, the wire EDM of SiC with the cutting direction a) parallel to the *c* axis showed a slightly higher area cutting speed compared with the cutting direction b) perpendicular to the *c* axis, as shown in Fig. 19 under the same machining conditions. Moreover, the EDMed surface topography of SiC along these two directions also differed considerably as shown in Fig. 20. Both machined surfaces presented a porous microstructure with fracture pits on them. However, large fracture pits were much less when the cutting direction was perpendicular to the *c* axis. The surface roughness R_z, however, presented no significant difference.

With regard to the reason for the differences in the machining rate and surface topography, the crack failure of SiC may have occurred more easily when the cutting direction was parallel to the crystal axis. On the other hand, it may have been caused by the thermal anisotropy properties of SiC single crystal. Wutimakun et al. (2008) reported that the thermal diffusivities of the <1–100> and <11–20> orientations (⊥*c* axis) were higher than those of the <0001> orientation (//*c* axis). Therefore, the heat conduction is lower in the direction parallel to the *c* axis, which results in a higher surface temperature in the EDM of SiC, consequently causing a higher probability of fractures.

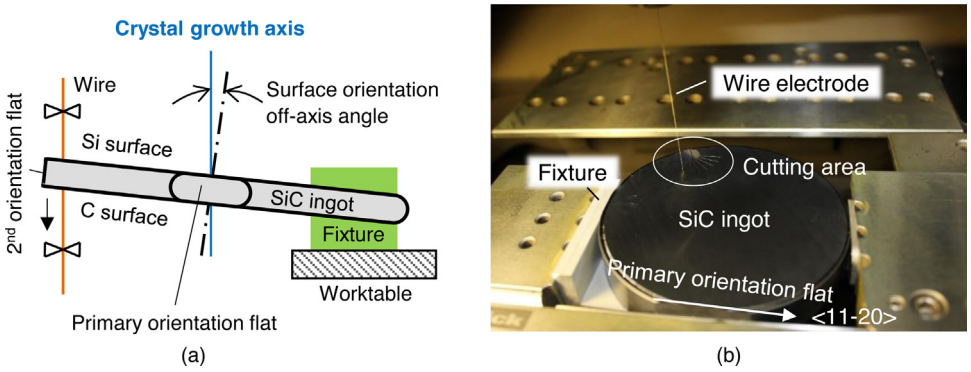

Fig. 17. Schematic diagram and image of experimental setup for wire EDM of SiC ingot.

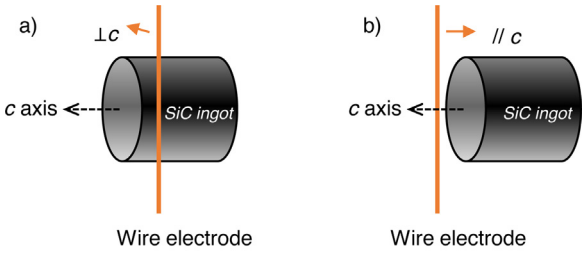

a) Perpendicular to c axis, b) parallel to c axis

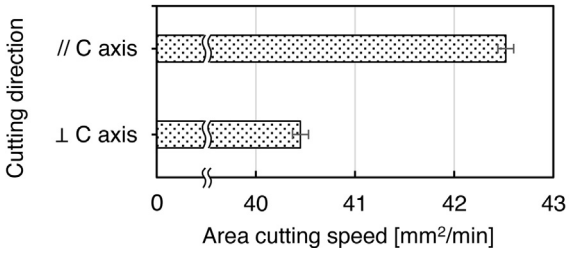

Fig. 19. Variation of machining rate along different crystal orientations.

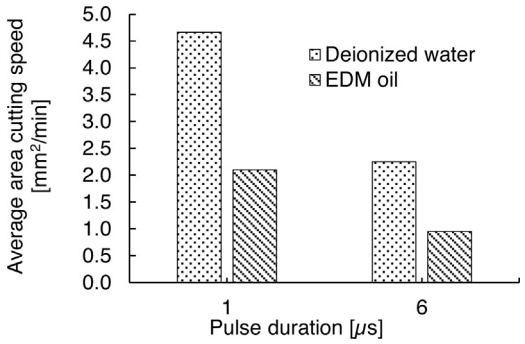

Fig. 21. Difference of machining rate caused by different dielectric fluids i_e = 14A).

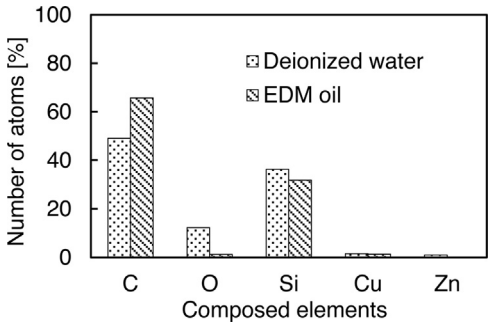

Fig. 22. Results of elemental analysis of EDMed surface of SiC by EDS.

5. Oxidation reaction

The EDM of SiC was compared between EDM oil and deionized water. Fig. 21 shows the difference in the machining rate under the same pre-set machining conditions. The average area cutting speed was approximately two times higher in deionized water than that in EDM-oil under both short and long pulse durations. With regard to the reason, oxidation reaction effect in deionized water was considered.

EDM is undeniably a thermal process. However, it is also acknowledged as a chemical process. Yu and Kunieda (1999) reported that oxidation of workpiece materials occurs when water-based dielectric is used because water can be dissociated by arc discharge into hydrogen and oxygen. To clarify the oxidation effect in the EDM of SiC in deionized water, the elemental composition of SiC surface after EDM in deionized water and oil was analyzed respectively by energy dispersive X-ray spectroscopy (EDS) under a scanning electron microscope (JEOL JSM-7001F). The analysis area of SiC surface was 1mm × 1 mm square. Fig. 22 shows the quantitative analysis results of the component elements of SiC. The existence of oxygen (O) was confirmed on SiC surface when machining in deionized water and the number of oxygen atoms accounted for around 15 percent of all the elements. On the other hand, little oxygen was found when the machining was conducted in oil. This confirmed the oxidation effect of the workpiece in the EDM of SiC by deionized water dielectric. Kunieda et al. (1991) investigated the influence of oxidation reaction in EDM by supplying oxygen gas into the discharge gap and found that a higher EDM rate can be obtained with the assistance of oxygen. According to their theory, oxidation reaction is an exothermic process capable of increasing the rate of heat generation in EDM, which is helpful for melting workpiece and increasing explosive force to remove the molten material. Therefore, the oxidation reaction in the EDM of SiC is considered to be another factor contributing to the improvement of the material removal rate. On the other hand, copper (Cu) and

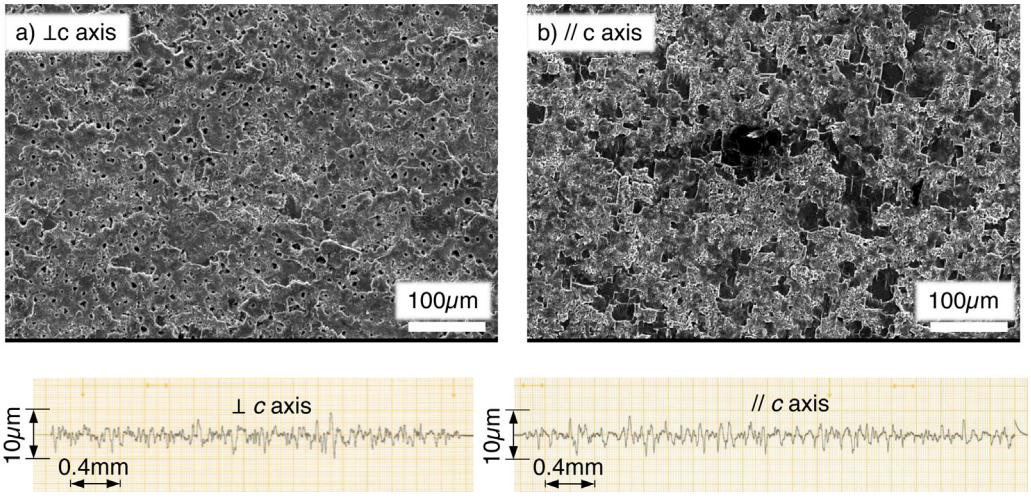

Fig. 20. Micro topography and surface roughness profile of wire EDMed surface of SiC. a) Cutting direction perpendicular to c axis; b) Cutting direction parallel to c axis.

zinc (Zn) were also detected on the SiC surface. This is due to the deposition of the melted tool electrode material (brass) on the SiC surface during machining.

6. Conclusions

The study investigated the EDM mechanism of single crystal SiC from thermal, mechanical and chemical aspect respectively. The results are summarized below:

1) The results of heat conduction analysis confirmed that the peak temperature on the workpiece surface was two times higher when Joule heating effects were present than when without, indicating that Joule heating effect contributes to the increase in the temperature of SiC near the discharge spot significantly. On the other hand, due to the extremely high thermal conductivity of SiC and the expansion of plasma diameter, the surface temperature dropped quickly below the decomposition point of SiC with the lapse of time after the discharge ignition. This explains why long pulse duration causes a lower machining efficiency in the EDM experiments of SiC compared with that of short pulse duration under the same duty factor.
2) With respect to single discharge, the area of high temperature region which exceeds the sublimation/decomposition point of SiC is several times larger than the area of high temperature region of steel which exceeds the melting point of steel. This could result in an improvement of the material removal rate of SiC as compared with that of steel.
3) Thermal cracks and fracture occurred in the EDM of SiC along crystal orientations which could improve the machining rate of SiC. Investigation on the influence of the crystal anisotropy on EDM performance showed that a slightly higher machining rate can be obtained when the cutting direction is along the *c* axis. Moreover, more fracture pits occurred on the machined surface when the cutting direction is parallel to the *c* axis of SiC.
4) The EDM of SiC in deionized water provided a higher machining rate than that in EDM oil. Twelve percent of oxygen was detected on the EDMed SiC surface in deionized water, indicating that oxidation effect is significant in the EDM of SiC in water, contributing to the higher EDM rate of SiC.

Acknowledgement

This research was supported by the Grant-in-Aid for Research Activity Start-up from JSPS (15H06138).

A part of this study was conducted in the collaborative research with Nippon Steel & Sumitomo Metal Corporation, Nippon Steel & Sumikin Materials Co., Ltd, and Sodick Co., Ltd.

In addition, a part of this study was supported by the "Nanotechnology Platform Project" (Project No. 12024046) of the Ministry of Education, Culture, Sports, Science and Technology (MEXT), Japan.

References

Dhanaraj, G., Byrappa, K., Prasad, V., Dudley, M., 2010. Springer Handbook of Crystal Growth. Springer, Berlin, Heidelberg.
Emsley, J., 1998. The Elements, third edition. Oxford University Press, pp. 1998.
Friedrichs, P., Kimoto, T., Ley, L., Pensl, G., 2010. Silicon Carbide 2: Power Devices and Sensors. Wiley-VCH Verlag GmbH&Co. KGaA, Weinheim.
Ishikawa, Y., Yao, Y., Sugawara, Y., Sato, K., Okamoto, Y., Hayashi, N., Dierre, B., Watanabe, K., Sekiguchi, T., 2014. Comparison of slicing-induced damage in hexagonal SiC by wire sawing with loose abrasive, wire sawing with fixed abrasive, and electric discharge machining. Jpn. J. Appl. Phys. 53 (7), 071301.
Itokazu, A., Miyake, H., Hashimoto, T., Fukushima, K., 2014. Multi-wire electrical discharge slicing for silicon carbide Part 2: Improvement on manufacturing wafers by forty-wire EDS. Mater. Sci. Forum 778–780, 763–766.
Ji, R., Liu, Y., Zhang, Y., Cai, B., Li, H., Ma, J., 2010. Optimizing machining parameters of silicon carbide ceramics with ED milling and mechanical grinding combined process. Int. J. Adv. Manuf. Technol. 51 (1), 195–204.
Ji, R., Liu, Y., Zhang, Y., Wang, F., 2011. Machining performance of silicon carbide ceramic in end electric discharge milling. Int. J. Refract. Metals Hard Mater. 29 (1), 117–122.
Ji, R., Liu, Y., Zhang, Y., Cai, B., Li, X., Zheng, C., 2013. Effect of machining parameters on surface integrity of silicon carbide ceramic using end electric discharge milling and mechanical grinding hybrid machining. J. Mech. Sci. Technol. 27 (1), 177–183.
Kato, T., Noro, T., Takahashi, H., Yamaguchi, S., Arai, K., 2009. Characterization of electric discharge machining for silicon carbide single crystal. Mater. Sci. Forum 600–603, 855–858.
Kawakami, T., Kunieda, M., 2005. Study on factors determining limits of minimum machinable size in micro EDM. CIRP Annal. – Manuf. Technol. 54 (1), 167–170.
Kitamura, T., Kunieda, M., 2014. Clarification of EDM gap phenomena using transparent electrodes. CIRP Annal. – Manuf. Technol. 63 (1), 213–216.
Kitamura, T., Kunieda, M., Abe, K., 2013. High-speed imaging of EDM gap phenomena using transparent electrodes. Procedia CIRP 6, 314–319.
Kojima, A., Natsu, W., Kunieda, M., 2008. Spectroscopic measurement of arc plasma diameter in EDM. CIRP Annal. – Manuf. Technol. 57 (1), 203–207.
Kunieda, M., Furuoya, S., Taniguchi, N., 1991. Improvement of EDM efficiency by supplying oxygen gas into gap. CIRP Annal. – Manuf. Technol. 40 (1), 215–218.
Kunieda, M., 2014. Electrical Discharge Machining Processes, Handbook of Manufacturing Engineering and Technology. Springer-Verlag, London, pp. 1551–1580.
Lauwers, B., Kruth, J.P., Liu, W., Eeraerts, W., Schacht, B., Bleys, P., 2004. Investigation of material removal mechanisms in EDM of composite ceramic materials. J. Mater. Process. Technol. 149 (1–3), 347–352.
Liu, Y., Ji, R., Li, Q., Yu, L., Li, X., 2008. Electric discharge milling of silicon carbide ceramic with high electrical resistivity. Int. J. Mach. Tools Manuf. 48 (12–13), 1504–1508.
Luis, C., Puertas, I., Villa, G., 2005. Material removal rate and electrode wear study on the EDM of silicon carbide. J. Mater. Process. Technol. 164–165, 889–896.
Matsunami, H., Otani, N., Kimoto, T., Nakamura, T., 2011. Technology of Semiconductor SiC and Its Application. Nikkan Kogyo Shimbun Ltd., pp. 100–112 [In Japanese].
Ogawa, M., Mine, K., Fuchiyama, S., Tawa, Y., Kato, T., 2014. Development of multi-wire electric discharge machining for SiC wafer processing. Mater. Sci. Forum 778–780, 776–779.
Okamoto, Y., Kimura, A., Okada, A., Uno, Y., Ohya, J., Yamauchi, T., 2012. Challenge to development of functional multi-wire EDM slicing method using wire electrode with track-shaped section. Key Eng. Mater. 523–524, 287–292.
Rich, J.A., 1961. Resistance heating in the arc cathode spot zone. J. Appl. Phys. 32 (6), 1023–1031.
Saeki, T., Kunieda, M., Ueki, M., Satoh, Y., 1996. Influence of Joule heating on EDM processes of high-electric-resistivity materials. ASME HTD (Am. Soc. Mech. Eng. Heat Transf. Div.) 366, 95–103.
Saito, N., Kobayashi, K., 1967. Machining principle and characteristics of electric discharge machining. Mitsubishi Denki Giho 41 (10), 1222–1230 (In Japanese).
Syvajarvi, M., Yakimova, R., Janzen, E., 2000. Cross-sectional cleavages of SiC for evaluation of epitaxial layers. J. Cryst. Growth 208 (1–4), 409–415.
Wutimakun, P., Miyazaki, H., Okamoto, Y., Morimoto, J., Hayashi, T., Shiomi, H., 2008. Studies of thermal anisotropy in 4H- 6H-SiC bulk single crystal wafers by photopyroelectric (PPE) method. Mater. Sci. Forum 600–603, 521–524.
Xia, H., Kunieda, M., Nishiwaki, N., 1996. Removal amount difference between anode and cathode in EDM process. Int. J. Electr. Mach. 1, 45–52.
Yamada, H., Yamaguchi, S., Yamamoto, N., Kato, T., 2012. Cutting speed of electric discharge machining for SiC ingot. Mater. Sci. Forum 717–720, 861–864.
Yamashita, M., Kitamura, T., Yamashita, K., Fukuzawa, Y., 2011. Effect of the material properties on removal rate in SEDM. J. Jpn. Soc. Electr. Mach. Eng. 45 (109), 71–79 (in Japanese).
Yan, J., Tan, T., 2015. Sintered diamond as a hybrid EDM and grinding tool for the micromachining of single-crystal SiC. CIRP Annal. – Manuf. Technol. 64 (1), 221–224.
Yu, Z., Kunieda, M., 1999. Study on material removal rate of EDM in deionized water. J. Jpn. Soc. Electr.-Mach. Eng. 33 (72), 28–36 (in Japanese).
Zhao, Y., Kunieda, M., Abe, K., 2014. Study of EDM cutting of single crystal silicon carbide. Precis. Eng. 38 (1), 92–99.
Zhao, Y., Kunieda, M., Abe, K., 2015. Multi-discharge EDM coring of single crystal SiC ingot by electrostatic induction feeding method. Precis. Eng. 41, 24–31.